International Journal of Electrical and Electronic Engineering & Telecommunications

ISSN 2319 – 2518 www.ijeetc.com
Vol. 3, No. 2, April 2014

Research Paper

MODELLING AND APPLICATION OF TRANSFER FUNCTION ANALYSIS FOR ENERGY-EFFICIENT DYNAMIC DRIVE CONTROL (WIND POWER MODELING)

M Gopichand Naik[1] and M Rakesh[1]*

*Corresponding Author: ***M Rakesh,*** ✉ *hiboss46@gmail.com*

There is, however, abundant inertial resources in wind plant rotors for both smoothing of output power and for inertia contribution. Where as with added frequency controlling drive, this could facilitate inclusion of wind power in islanding systems, enabling greater system loads and enhancing power system stability. Modeling of power smoothing and frequency controlling wind plants and access different control strategies. this indicates that the manufacturer maximum blade pitch rate affects the frequency controlling performance this paper suggest that the control architecture in the wind plants be kept as simple as possible, involving only modifications of the algorithms in the speed controller. The results shown in output could be smoothed in the short time frame. The synthesis of a power control loop to closely follow maximum available wind power is performed based on the design rules. In this context, the voltage sourced converter is operated in current mode control to contribute to fast adjustment of air-gap torque while maintaining currents within limits. The direct and quadrature current references are calculated to attain the desired torque at minimal stator current magnitude and so enhance energy efficiency. The dynamic performance of the design is evidenced by time-domain simulation and stochastic analysis.

Keywords: Pitch control, Frequency control, FPCWT, Inertia, PMSG, Power smoothing, Primary frequency control, Wind power, Power smoothing

INTRODUCTION

The rising share of wind energy with its implications for power system operation calls for a profound understanding of the static and dynamic behaviour and controls of Wind Energy Conversion Systems (WECS). Power electronic control adopts a key role in modifying the behaviour of the different WECS

[1] Department of Electrical Engineering, AUCE (A), Visakhapatnam, India.

technologies. Examples for such control functions in normal operation include optimal power tracking under various conditions or the smoothing of power fluctuations.

For wind energy converters with Permanent Magnet Synchronous Generators (PMSG), linearization has been applied in the formulation of state-space representations to perform Eigen value analysis and assess stability limits. What is critically missing, however, are transfer function descriptions of the machine side that readily identify how all critical parameters of turbine, generator, and power electronic control impact dynamic behaviour and stability. This is where the contributions of this paper come in. First, the machine side of a WECS is structured into the three functional stages of power synthesizer controller, current vector optimizer-controller together with torque generation, as well as turbine-rotor interaction process.

Within these functional stages, rigorous decompositions lead to well-defined blocks of power conversion and controls. For the PMSG, optimization is applied to yield minimal current amplitude and minimal resistive losses at a given air-gap torque. Second, compacted and illustrative transfer functions are formulated to readily identify associated poles and zeros pertaining to all functional stages. Such transfer functions have proven valuable in electric motor drive analysis. A major difference here is the integration of the wind turbine characteristics. It will become clear how different wind speeds and rotor angular velocities affect dynamic performance and stability considering transfer function poles and zeros. Control parameter setting rules are developed for integral and lead-lag compensators. Third, a case study puts into evidence the validity and applicability of the proposed transfer functions and controller setting rules. While the descriptions focus on WECS with direct-drive PMSG and fully rated converters, the methods can also be readily adapted to WECS with gearbox or synchronous generators with electrical excitation.

Over All Block Diagram

The wind at velocity V_w leads to an accelerating torque T_{tur} on the shaft through action of the turbine. The mechanical angular velocity of the rotor is equal to the electrical angular velocity ωe 2× and divided by the number of poles p. The electromagnetic air-gap torque coming from the PMSG has a decelerating effect as the PMSG delivers electric power through the Voltage Sourced Converter (VSC). The direction and signs given for the three-phase stator voltages and currents shown between the blocks of PMSG and VSC follow the generator convention. Power delivered by the PMSG is counted positive in generator mode. On the dc side, the VSC is connected to a dc bus. Further resources may also be connected to the dc bus. A connection to the ac electric power grid is established through a dc–ac power electronic converter. The controls of this converter keep the dc voltage at the desired value. The three-phase voltages and currents in the circuit have already been converted into *dq*-variables as a first step in this direction. This can readily be appreciated from the inputs and outputs of the PMSG. The latter is separated into three blocks pertaining to electrical, electromagnetic, and mechanical stages. In the following sections, the underlying equations will be rearranged to give a compact description and then literalized to allow for

application of linear control theory and enhanced insight into system behaviour of the drive. The sections follow the decomposition into three functional stages:

1. Power synthesizer-controller;
2. Current vector optimizer-controller and torque generation; and
3. Turbine-rotor interaction process.

CURRENT VECTOR OPTIMIZER, CONTROLLER, AND TORQUE GENERATION

In this section, it is first reviewed how the electric system consisting of generator and VSC can be modelled by considering existing literature knowledge. It is discussed how a second-order closed current control loop representation based on transfer functions is obtained. Then, a small-signal linearized formulation of the optimization for minimal stator current at a given torque is obtained.

Electric System Modelling

The stator equations are commonly expressed in a *dq*-frame that rotates at the electrical angular velocity ωe of the rotor. The *d*-axis is magnetically cantered on the North Pole, and the *q*-axis leads the *d*-axis by 90°. The generator mode convention with the direction of positive stator currents i_{sd} and i_{sq} out of the generator is applied

$$v_{sd} = L_{sq}.i_{sq}.w_e - L_{sd}.\frac{di_{sd}}{dt} - R_s i_{sd} \quad ...(1)$$

$$v_{sq} = (\phi_m - L_{sd}.i_{sd}).w_e - L_{sq}.\frac{di_{sq}}{dt} - R_s i_{sq} \quad ...(2)$$

where v_{sd} and v_{sq} are the *d*-axis and *q*-axis stator terminal voltages; L_{sd} and L_{sq} are the *d*-axis and *q*-axis stator inductances that are, respectively, composed of magnetizing and leakage inductances, *_m* gives the amplitude of the magnetic flux linkage caused by the rotating permanent magnet in the stator, and *Rs* is the resistance of the stator phase windings. The stator terminal voltages are obtained from the VSC and depend on the modulating signals and the dc voltage. On the dc side, the voltage is tapped to the reference node at the midpoint leading to a plus terminal +(*vdc*/2) and a minus terminal –(*vdc*/2). Considering the assumptions and further derivations of Appendix B, the VSC model is as follows:

$$v_{sd} = m_d \frac{v_{dc}}{2} \quad ...(3)$$

$$v_{sq} = m_q \frac{v_{dc}}{2} \quad ...(4)$$

$$i_{dc} = \frac{3}{4}(m_d.i_{sd} + m_q.i_{sq}) \quad ...(5)$$

Current Control Loop

The modulating signals md and mq are produced by the current controller. Designing the current controller, it is important to understand the stator dynamics. For that purpose, (1) and (2) can be rewritten in the Laplace domain when neglecting initial conditions as

$$i_{sd} = -\frac{1}{R_s + sL_{sd}}(v_{sd} - L_{sq}.i_{sq}.w_e) \quad ...(6)$$

$$i_{sq} = -\frac{1}{R_s + sL_{sq}}(v_{sd} - (\phi_m - L_{sq}.i_{sq}).w_e) \quad ...(7)$$

Both equations are coupled. It is common practice to decouple the respective control

Figure 1: Entire Block Diagram

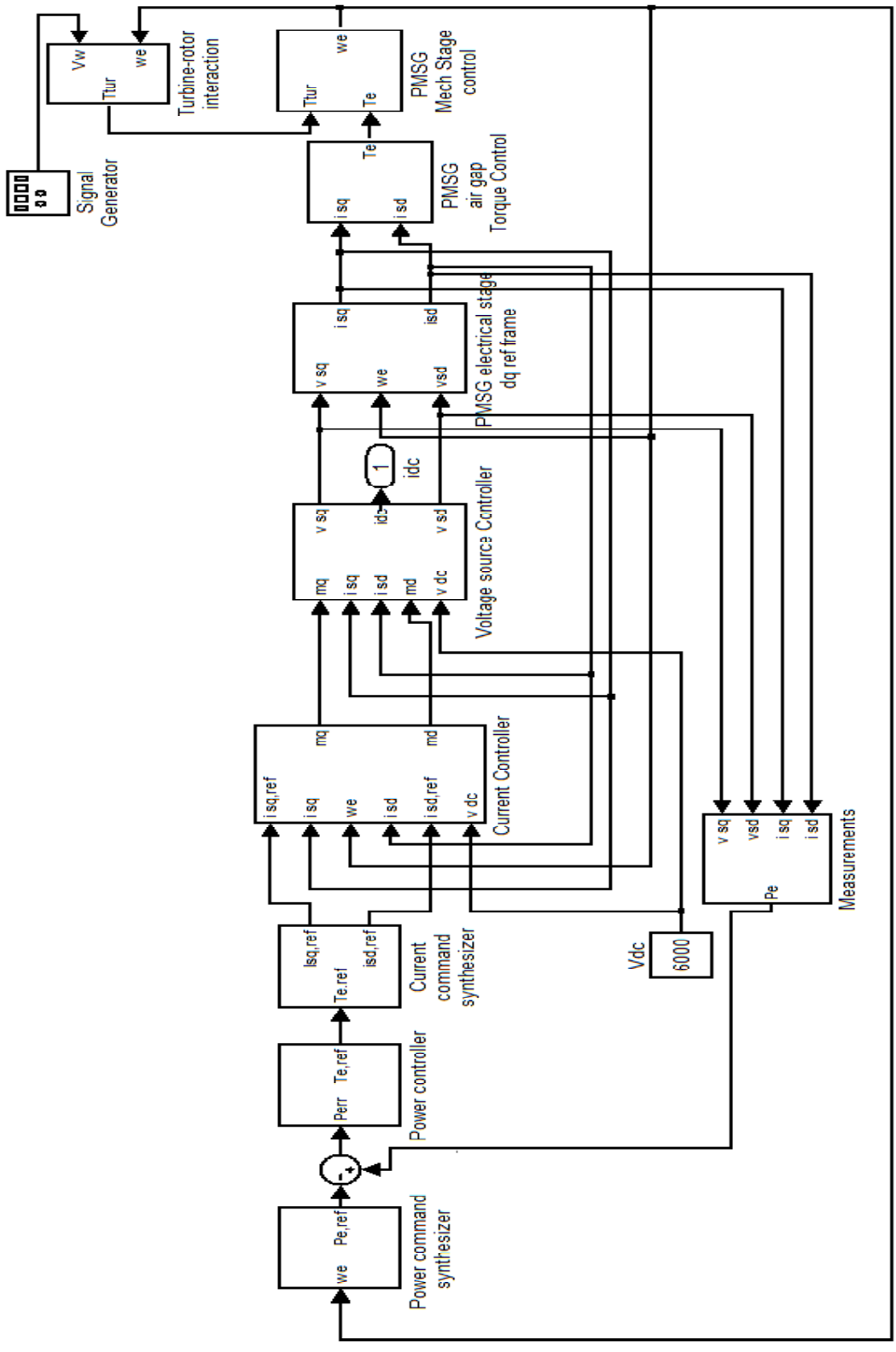

loops by definition of substitute control variables

$$y_d = v_{sd} - L_{sq}.i_{sq}.w_e \quad ...(8)$$

$$y_q = v_{sq} - (\phi_m - L_{sd}.i_{sd}).w_e \quad ...(9)$$

These substitute control variables appear as outputs of the controller compensation functions $G_{id}(s)$ and $G_{iq}(s)$. The latter have the current errors appear as inputs

$$y_d = G_{id}(s)(i_{sq,ref} - i_{sq}) \quad ...(10)$$

$$y_q = G_{iq}(s)(i_{sd,ref} - i_{sd}) \quad ...(11)$$

$$G_{id}(s) = K_{d,P} + \frac{K_{d,I}}{s} \quad ...(12)$$

$$G_{iq}(s) = K_{q,P} + \frac{K_{q,I}}{s} \quad ...(13)$$

Air-Gap Torque

The electromagnetic torque generated in the air-gap of the PMSG is given by

$$T_e = \frac{3}{2}.\frac{p}{2}(\phi_m i_{sq} - (L_{sd} - L_{sq}) i_{sd} i_{sq}) \quad ...(14)$$

where T_e gives positive values for generator mode. Equation (14) represents the block of the PMSG electromagnetic stage.

Current Command Synthesizer

As shown in Figure 1, the torque reference coming from the power controller is decomposed into current references by the current command synthesizer. Based on a given reference for T_e, it is desirable to select the current vector references composed of i_{sd}, ref and i_{sq}, ref such that the magnitude $|i_s|$ is minimized. This implies that the stator resistive losses are minimized and contributes so to the energy efficiency of the overall plant.

$$i_{sd,\,ref} = \frac{-T_{e,ref}}{\frac{3}{2}.\frac{p}{2}(L_{sd} - L_{sq}) i_{sq,\,ref}} + \frac{\phi_m}{(L_{sd} - L_{sq})} \quad ...(15)$$

$$i_{sq,\,ref} = \frac{\frac{8}{3p} T_{e,ref} - \phi_m . i_{sq,\,ref}}{4.i_{sq,\,ref}^{\,3} \frac{3}{2}.\frac{p}{2}(L_{sd} - L_{sq})^2 + \phi_m . T_{e,ref}} \quad ...(16)$$

TURBINE-ROTOR INTERACTION PROCESS

Assuming a rigid drive train, the equation of motion is given by

$$J \frac{2}{p} \frac{dw_e}{dt} = T_{tur} - T_e - T_d \quad ...(17)$$

Here, p is the number of poles of the PMSG, and T_d can give damping due to friction. The aerodynamic torque T_{tur} of the wind turbine is given by

$$T_{tur} = \frac{1}{2} \pi \rho r^3 V_w^2 C_T(\lambda) \quad ...(18)$$

with the tip speed ratio

$$\lambda = \frac{dw_m r}{V_\omega} \quad ...(19)$$

where ρ is the air density, r is the blade length, V_w is the wind velocity, ωm is the mechanical angular velocity, and $C_T(\lambda)$ is the torque coefficient. For limited excursions about a steady-state operating point, the torque coefficient may be approximated through a second order polynomial

$$C_T = c_0 + c_1\lambda + + c_2\lambda^2 \quad ...(20)$$

$$C_T(\lambda) = C_P(\lambda)/\lambda \quad ...(21)$$

Figure 2: Block Diagram of Current Control

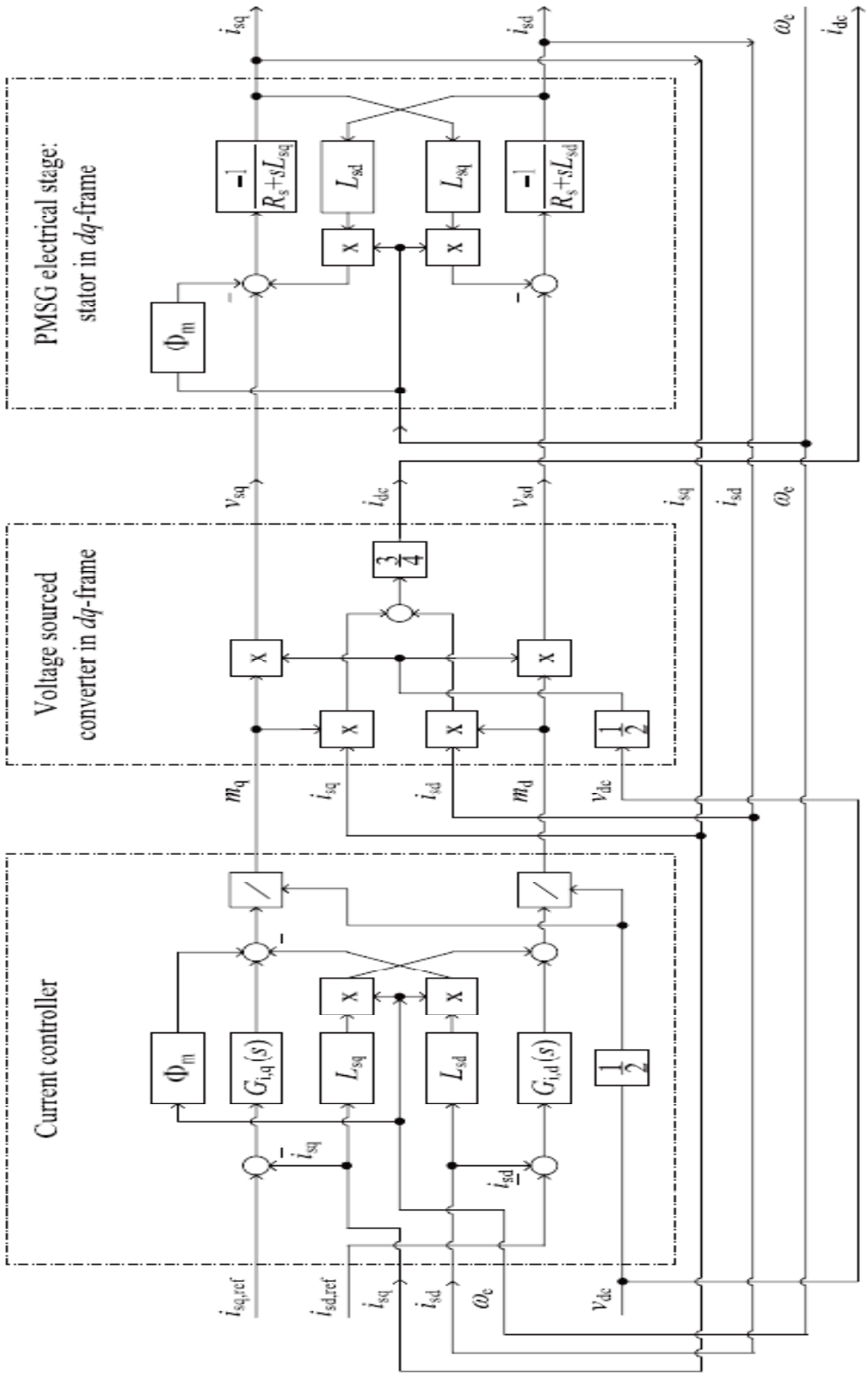

Figure 3: Power Coefficient $C_P(\lambda)$ and Torque Coefficient $C_T(\lambda)$

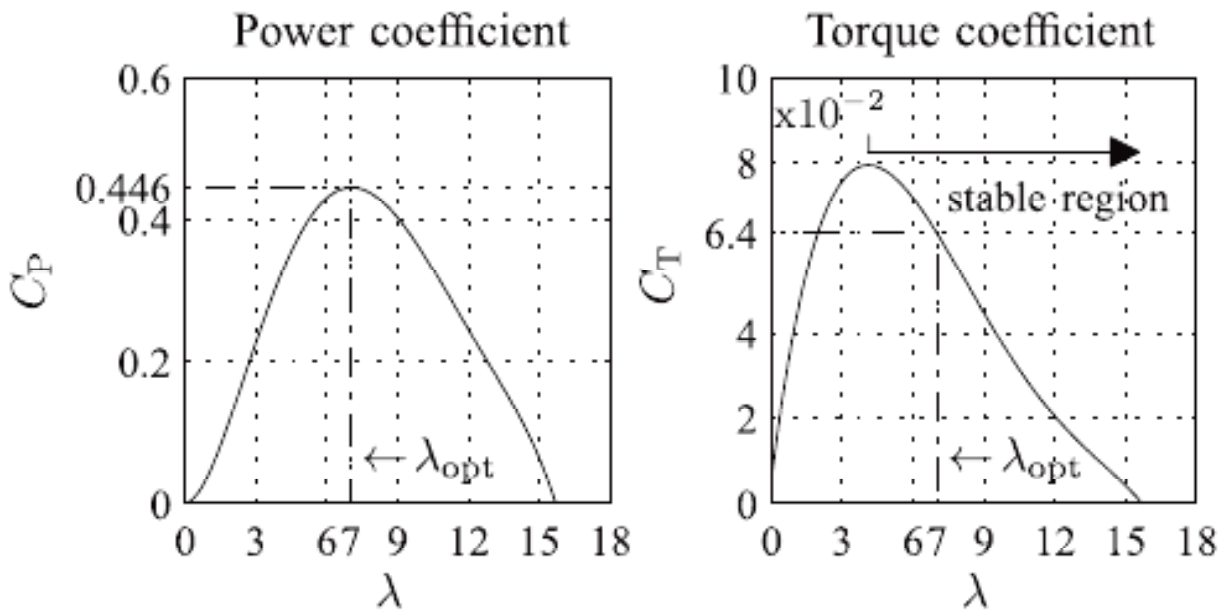

$$P_e = 2/p.T_e.\omega \quad ...(22)$$

POWER SYNTHESIZER

For a given wind speed, the maximum power that can be extracted by a turbine is given by

$$P_{tur} = \tfrac{1}{2}(\pi.\rho.r^2.V^3w.C_P(\lambda)) \quad ...(23)$$

The power coefficient $C_P(\lambda)$ relates to torque coefficient $C_T(\lambda)$ by $C_P(\lambda) = C_T(\lambda)\lambda$ and reaches its maximum at λ_{opt}.

$$P_{tur,opt} = \frac{4}{p^3}\pi\rho r^5 w_e^3 \frac{C_P(\lambda_{opt})}{\lambda_{opt}^3} \quad ...(24)$$

Neglecting the impact of mechanical power losses, this is the maximum power that can be transferred to the air-gap and is taken as a reference power of P_e to support energy efficiency

$$P_{e,ref} = P_{tur,opt} \quad ...(25)$$

Angular velocity ωe is the only time-varying quantity that $P_{tur,opt}$ depends on at $\lambda = \lambda_{opt}$. The reference is compared with the measured electric power, and the difference is fed to the power controller. The power delivered over the terminal of the PMSG is calculated from the terminal currents and voltages

$$P_{ter} = 3/2(vsd.isd + vsq.isq) \quad ...(26)$$

$$P_e = P_{ter} + P_R + P_L \quad ...(27)$$

CONTROLLER DESIGN

The block diagrams of the compacted linearized control loops are well suited for the design of controllers. In the turbine-rotor interaction process of the power control loop, it is assumed that $\tau\omega > 0$, $\tau z > 0$. The integral plus lead-lag compensator $G_P(s)$ proposed for this loop is of the following format:

$$G_P(s) = \frac{K(1+s\tau_{1e})}{s(1+s\tau_{1g})} \quad ...(28)$$

The lag and lead time constants τ_{lg} and τ_{le} are introduced to compensate the process

behaviour due to τz and $\tau \omega$. As the process is stable, pole-zero cancelation can be performed. The process pole is compensated by choosing

$$\tau_{1g} = \tau_{1e} \quad ...(29)$$

the process zero is compensated by setting.

The time constant of the closed loop can then be approximated by

$$\tau_{P1} = \frac{1.p.\tau_z}{K.2w_e.\tau_w} \quad ...(30)$$

$$K = \frac{1.p.\tau_z}{\tau_{P1}.2w_e.\tau_w} \quad ...(31)$$

Speed Controller

A decisive feature of the speed controller is the addition of the frequency signal after the original power order has been computed. In this way, the low pass power order filter ensures a steady power output during normal circumstances but does not obstruct fast response from the controller when grid disturbances occur. The controller design with low pass power order filtration removes rapid power changes and instead injects or subtracts kinetic energy to or from the rotor. One challenge of this strategy is the potential of brakeing the turbine rotor to a full stop when it is already under-speeded at the onset of a frequency disturbance. Rapidly decaying winds could cause such an initial condition. Implementation of a linear weighting of the frequency signal from 1 at full speed to 0 at 40% speed solves this problem, but at the same time also removes frequency responsive behavior below 6% power output which is the power output at 40% speed. The speed curve is a second-degree polynomial of speed as a function of power, injective from 0 to 1 p.u. produced power. This curve could have been shifted towards higher speed for delta pitch angles, but is kept identical to that of 0 pitch for simplicity. There is also an inherent power smoothing effect of operating with a lower than optimal in delta mode. Decreasing winds temporarily increase towards the optimal value and thereby increase Cp, and increasing winds temporarily decrease and thereby Cp, which means that the power output will be smoother than with initial operation at optimal lambda. The downside is that the recovery time after load steps will be longer due to the lower pre fault speed and thus a resulting lower post fault speed and lower which together cater for less aerodynamic lift to speed up the plant.

Pitch Controller

The pitch controller utilizes an identical frequency controller as that of the speed controller, but the parameterization is different, aiming at fast pitching response for small frequency errors. The desired functionality is an aggressive pitch controller that reaches early the maximum allowable pitch rate, 5 per second, facilitating quick changes in captured power. The pitch controller also holds the key function of the delta control as it is in the pitch

Figure 4: Modified Pitch Controller with Input Signals

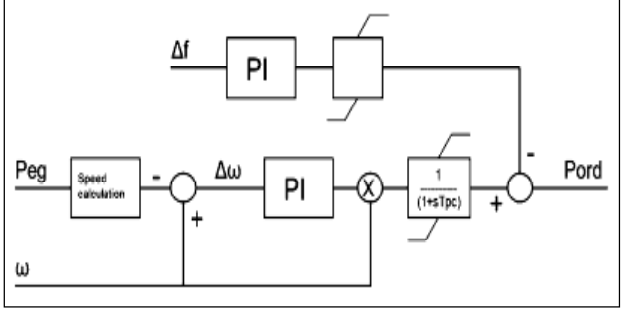

that the blade degree offset is introduced in the form of a constant addition to the normal pitch signal.

Figure 5: Controller Connection

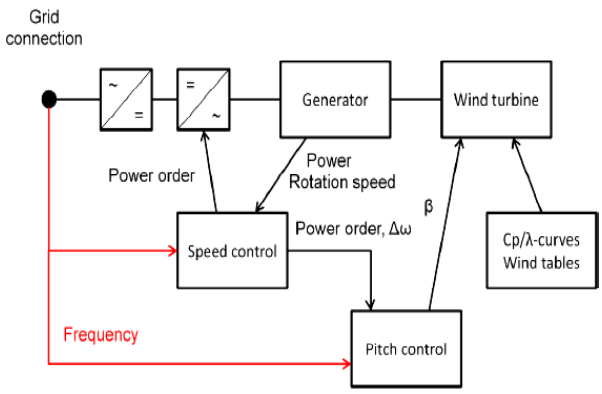

SIMULATION RESULTS

The validation of the design in following the maximum power points is made for a wind speed varying around an average of 9 m/s. The wind speed series is depicted on the top. This is followed by the air-gap torque, the stator current *q*-axis and *d*-axis components.

Figure 6: Wind Speed and Air Gap Torque

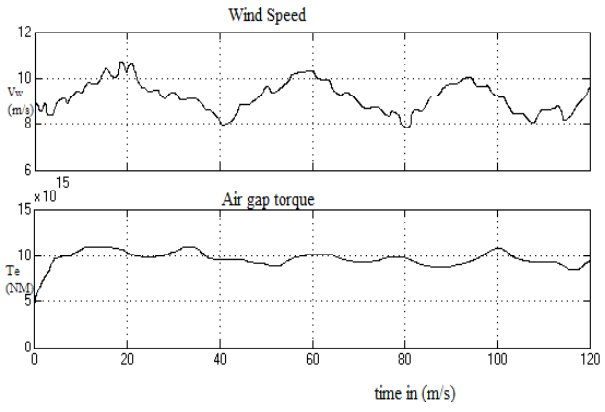

In Figure 8 on the left, the power coefficient CP is plotted versus the air-gap torque for the same interval of 10 min. The narrow range within which the maximum CP,opt is being tracked is well observed by the distribution on

Figure 7: Pe vs Perr

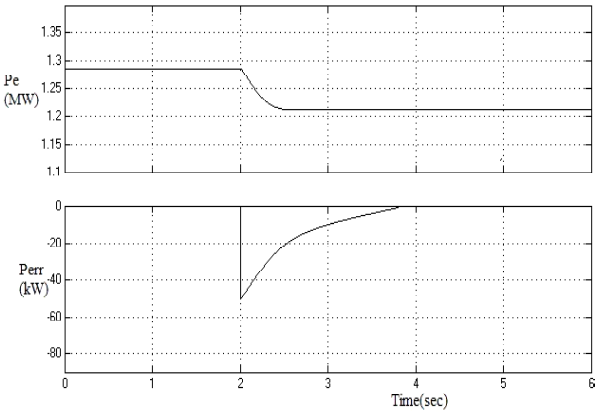

Figure 8: Power Tracking and Power Coefficients

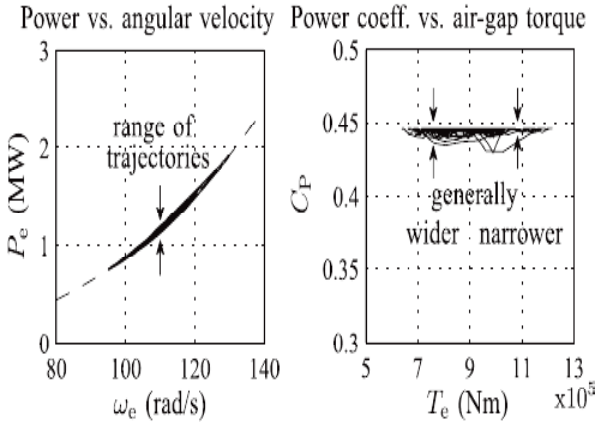

the right. A closer look at the C_P versus T_e plot reveals that around $Te = 10^6$ the range of C_P is generally narrower than at the lower $T_e = 8.10^5$. This observation is consistent with the statement that the gain of the process raises with the wind speed. Tracking is so improved at higher wind speeds for the same compensator settings.

Damping due to mechanical friction was neglected. The following parameters are valid for the operating point of the simulation at V_w = 9 m/s: P_{tur} = 1.27 MW, n = 13.5 rpm, and T_e = $8.95.10^5$ Nm. Coefficients for the second-order polynomial approximating the C_T curve around

Figure 9: Power Using Delta Controller

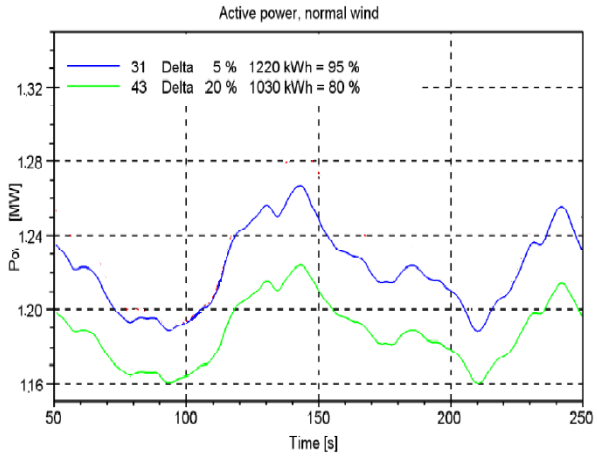

Figure 10: Dead Band Power Oscillations

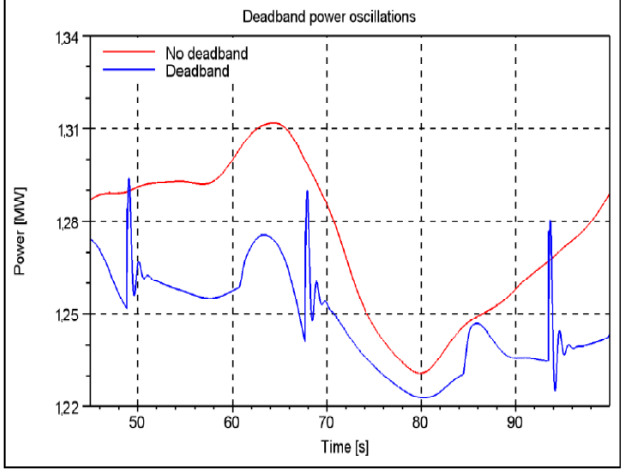

Figure 11: Frequency Without and with Dead Band

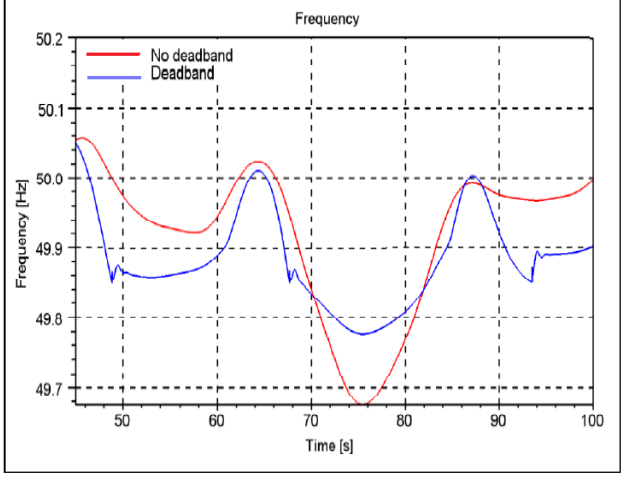

Table 1: Wind Turbine Parameters

Symbol	Quantity	Value
P_{tur}	Rated Power	3 MW
V_w	Rated Wind Speed	12 m/s
n	Rated Rotor Speed	18 rpm
$C_{P,opt}$	Maximum Power Coefficient	0.446
r	Rotor Radius	45 m
λ_{opt}	Optimal Tip Speed Ratio	7
H	Inertia Constant of Turbine and PMSG	5 s

Table 2: PMSG Parameters

Symbol	Quantity	Value
p	Number of Poles	160
R_s	Stator Resistance	50 mΩ
L_{sd}	Stator *d*-axis Inductance	4 mH
L_{sq}	Stator *q*-axis Inductance	6 mH
Φ_m	Flux Induced by Magnets	16.2 Wb

the operating point at $\lambda = 7$, $c_0 = 2.25.10^{-2}$, $c_1 = 2.18.10^{-2}$, and $c_2 = -0.23.10^{-2}$. The current control parameters are set such that $\tau i = 2$ ms. The *dc* voltage is *vdc* = 6 kV.

CONCLUSION

The overall methodology is distinguished by three contributions. First, the machine-side WECS was structured into block diagram format clearly identifying the various stages of power conversion and control. Linearization was applied to support small-signal analysis across all stages. It was shown how the phase-lead transfer function relating torque and power is influenced by wind speed and angular velocity of the rotor. The VSC connected to the generator is operated in current mode control. Second, the transfer functions have been arranged into a compact format such that they provide an intuitive framework for control system design. Locations of poles and zeros

and stability are identified, and an integral plus lead-lag compensator is designed for power control. The established design rules readily allow for adaptive compensator tuning depending on the operating point. This was evidenced by the design of the drive control system for energy efficiency. The control tracks maximum available wind power dynamically while at the same time decomposing the stator current into direct and quadrature axis components for loss minimization. Third, large-signal time-domain simulation was performed to verify the design. A stochastic analysis leading to the distributions of power coefficient and deviation of the power from its maximum confirmed a close following of maximum power set point.

In sum, the contributions made offer a better and enhanced insight into the various parameters influencing the behaviour of wind energy conversion involving PMSG. This again has shown to be a valuable basis for compensator tuning making effective use of power electronics to control wind power converters for energy efficiency.

REFERENCES

1. Blaabjerg F and Ma K (2013), "Future on Power Electronics for Wind Turbine Systems", *IEEE J. Emerg. Sel. Topics Power Electron.*, Vol. 1, No. 3, pp. 139-152.
2. Brussels and Belgium (2012), "Global Wind Energy Council", Global Wind Report [Online], available http://www.gwec.net
3. Cardenas R, Pena R, Tobar G, Clare J, Wheeler P and Asher G (2009), "Stability Analysis of a Wind Energy Conversion System Based on a Doubly Fed Induction Generator Fed by a Matrix Converter", *IEEE Trans. Ind. Electron.*, Vol. 56, No. 10, pp. 4194-4206.
4. Liserre M, Cardenas R, Molinas M and Rodriguez J (2011), "Overview of Multi-MW Wind Turbines and Wind Parks", *IEEE Trans. Ind. Electron.*, Vol. 58, No. 4, pp. 1081-1095.
5. Manwell J F, McGowan J G and Rogers A L (2002), *Wind Energy Explained*, Wiley, New York, USA.
6. Polinder H, an der Pijl F F A, de Vilder G-J and Tavner P J (2006), "Comparison of Direct-Drive and Geared Generator Concepts for Wind Turbines", *IEEE Trans. Energy Convers.*, Vol. 21, No. 3, pp. 725-733.
7. Simoes M G and Farret F A (2008), "Alternative Energy Systems: Design and Analysis with Induction Generators", CRC Press, Cleveland, OH, USA.
8. Yazdani A and Iravani R (2006), "A Neutral-Point Clamped Converter System for Direct-Drive Variable-Speed Wind Power Unit", *IEEE Trans. Energy Convers.*, Vol. 21, No. 2, pp. 596-607.